| | |
|---|---|
| Title | Spin excitations in optimally P-doped $BaFe_2(As_{0.7}P_{0.3})_2$ superconductor |
| Author(s) | Hu D., Yin Z., Zhang W., Ewings R. A., Ikeuchi Kazuhiko, Nakamura Mitsutaka, Roessli B., Wei Y., Zhao L., Chen G., Li S., Luo H., Haule K., Kotliar G., Dai P. |
| Citation | Physical Review B,94(9),p.094504_1-094504_7 |
| Text Version | Publisher's Version |
| URL | https://jopss.jaea.go.jp/search/servlet/search?5057127 |
| DOI | https://doi.org/10.1103/PhysRevB.94.094504 |
| Right | © 2016 The American Physical Society |

# Spin excitations in optimally P-doped $BaFe_2(As_{0.7}P_{0.3})_2$ superconductor

Ding Hu,[1,2] Zhiping Yin,[1,3,*] Wenliang Zhang,[2] R. A. Ewings,[4] Kazuhiko Ikeuchi,[5] Mitsutaka Nakamura,[6] Bertrand Roessli,[7] Yuan Wei,[2] Lingxiao Zhao,[2] Genfu Chen,[2] Shiliang Li,[2,8] Huiqian Luo,[2] Kristjan Haule,[3] Gabriel Kotliar,[3,9] and Pengcheng Dai[10,1,†]

[1]*Center for Advanced Quantum Studies and Department of Physics, Beijing Normal University, Beijing 100875, China*
[2]*Beijing National Laboratory for Condensed Matter Physics, Institute of Physics, Chinese Academy of Sciences, Beijing 100190, China*
[3]*Department of Physics, Rutgers University, Piscataway, New Jersey 08854, USA*
[4]*ISIS Facility, STFC Rutherford Appleton Laboratory, Harwell Campus, Didcot OX11 0QX, United Kingdom*
[5]*Research Center for Neutron Science and Technology, Comprehensive Research Organization for Science and Society (CROSS), Tokai, Ibaraki 319-1106, Japan*
[6]*Materials and Life Science Division, J-PARC Center, Tokai, Ibaraki 319-1195, Japan*
[7]*Laboratory for Neutron Scattering and Imaging, Paul Scherrer Institut, CH-5232 Villigen, Switzerland*
[8]*Collaborative Innovation Center of Quantum Matter, Beijing, China*
[9]*Brookhaven National Laboratory, Upton, New York 11973-5000, USA*
[10]*Department of Physics and Astronomy, Rice University, Houston, Texas 77005, USA*

(Received 13 February 2016; revised manuscript received 26 July 2016; published 2 September 2016)

We use inelastic neutron scattering to study the temperature and energy dependence of spin excitations in an optimally P-doped $BaFe_2(As_{0.7}P_{0.3})_2$ superconductor ($T_c = 30$ K) throughout the Brillouin zone. In the undoped state, spin waves and paramagnetic spin excitations of $BaFe_2As_2$ stem from an antiferromagnetic (AF) ordering wave vector $\mathbf{Q}_{AF} = (\pm 1,0)$, and peak near the zone boundary at $(\pm 1,\pm 1)$ around 180 meV. Replacing 30% As by smaller P to induce superconductivity, low-energy spin excitations of $BaFe_2(As_{0.7}P_{0.3})_2$ form a resonance in the superconducting state and high-energy spin excitations now peak around 220 meV near $(\pm 1,\pm 1)$. These results are consistent with calculations from a combined density functional theory and dynamical mean field theory, and suggest that the decreased average pnictogen height in $BaFe_2(As_{0.7}P_{0.3})_2$ reduces the strength of electron correlations and increases the effective bandwidth of magnetic excitations.

DOI: 10.1103/PhysRevB.94.094504

## I. INTRODUCTION

Since the discovery of unconventional superconductivity in iron pnictides near antiferromagnetic (AF) instability [1–7], a central issue has been whether these materials are fundamentally different from copper oxide superconductors, where the magnetism and superconductivity are derived from Mott physics and its associated electron correlations [8–14]. Since iron pnictides have tetrahedrally coordinated nearest pnictogen atoms, the $3d$ level in Fe ions splits into an $e_g$ state and a few hundred meV higher $t_{2g}$ state [15–22]. Without Hund's rule interaction, the $e_g$ state would be fully occupied with four of the six Fe $3d$ electrons while the remaining two $3d$ electrons should reside in the $t_{2g}$ state crossing the Fermi level. The presence of a strong Hund's coupling $J_H$, which tends to align spins of all the electrons on a given Fe atom, competes with the crystal field splitting and promotes high spin states of the Fe $3d$ electrons, resulting in large charge and spin fluctuations. Although it is generally accepted that electron correlations are also present in iron pnictides [11–14], it remains unclear if the correlation strength is controlled by the on-site Hubbard $U$ interaction as in the case of cuprates [8] or if it arises primarily from the Hund's coupling $J_H$ within one atomic site [15–17]. The local moments formed by the Fe $3d$ electrons, especially those in the $d_{xz}$, $d_{yz}$, and $d_{xy}$ orbitals, are coupled to their nearest neighbors by both the direct exchange associated with nearest-neighbor Fe-Fe distance and anisotropic superexchange interactions via hopping through the As pnictogen [Figs. 1(a)–1(c)]. By increasing the Fe-pnictogen distance, electron hopping between the nearest Fe ions becomes difficult, and the system is localized with enhanced electron correlations. On the other hand, reducing the Fe-pnictogen distance facilitates the electron hopping, thus reducing the electron correlations.

Using density functional theory (DFT) combined with dynamical mean field theory (DMFT) suitable for describing the Hund's coupling in iron pnictides [15–17,23,24], the evolution of spin excitations in electron- and hole-doped $BaFe_2As_2$ can be calculated [25–27]. In particular, the theory predicts that spin-wave and spin excitation bandwidths, defined as the peak in energy dependence of the dynamic susceptibility $\chi''(E)$ integrated near the AF zone boundary $(\pm 1,\pm 1)$ [25,27], in different iron pnictides are controlled by the iron-pnictogen distance and the valence of the Fe atoms similar to electron correlations [28]. Experimentally, spin waves and spin excitations in the electron- and hole-doped $AFe_2As_2$ ($A$ = Ba, Sr, Ca) family of iron pnictides mapped out by inelastic neutron scattering experiments throughout the Brillouin zone [29–33] are qualitatively consistent with the DFT+DMFT calculations and peak around 180 meV near (1,1) [25,27]. Although neutron scattering experiments on spin waves of NaFeAs, which has a larger pnictogen height ($h_{Pn} = 1.416$ Å) [34] compared with that of $BaFe_2As_2$ [Fig. 1(b), $h_{Pn} = 1.36$ Å], confirm the notion that increasing pnictogen height in iron pnictides decreases the spin-wave bandwidths to ∼110 meV near (1,1) and increases the electron correlation

*yinzhiping@bnu.edu.cn
†pdai@rice.edu

 

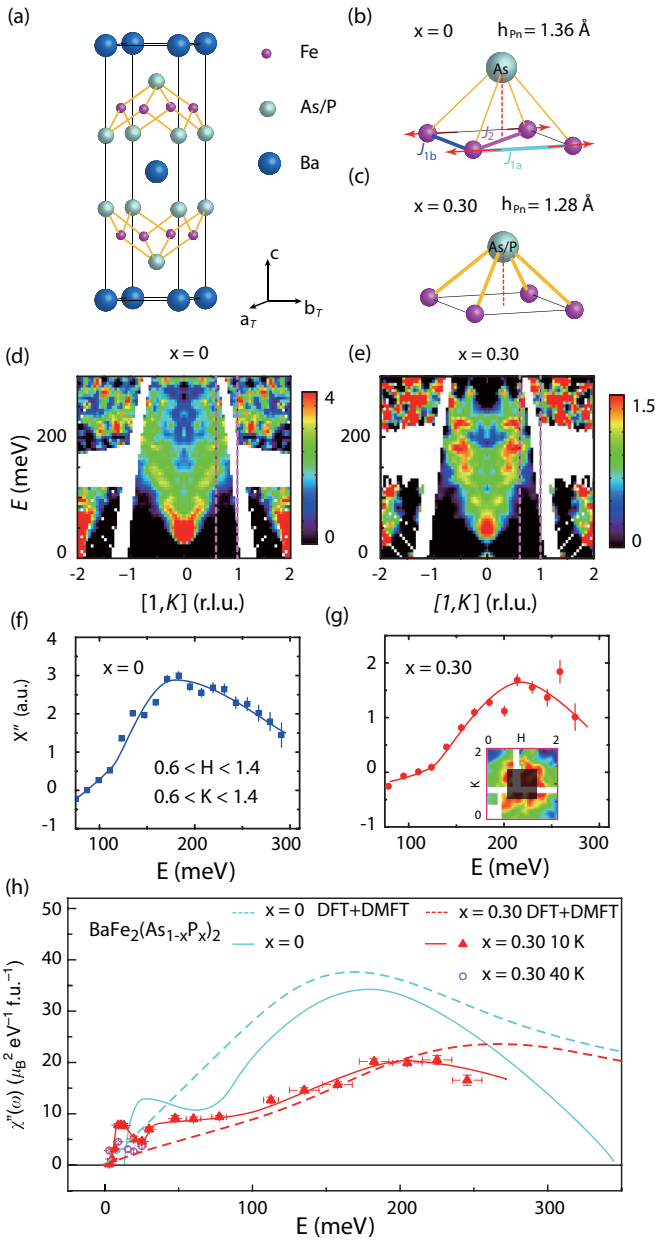


FIG. 1. (a) The crystal structure of $BaFe_2(As_{1-x}P_x)_2$. The purple, silvery, and blue balls indicate Fe, As/P, and Ba positions, respectively. (b), (c) Schematic diagrams of the FeAs tetrahedron, showing the average iron-pnictogen height decreased from 1.36 Å for $BaFe_2As_2$ to 1.28 Å for $BaFe_2(As_{0.7}P_{0.3})_2$ [37]. (d) The energy dependence of $S(Q,E)$ of spin waves of $BaFe_2As_2$ along the $(1,K)$ direction (with integration of $H$ from 0.9 to 1.1 r.l.u.) after subtracting the background integrated from $1.8 < H < 2.2$ and from $-0.25 < K < 0.25$ r.l.u. with $E_i = 450$ meV at $T = 10$ K measured on MAPS [30]. (e) Identical projection for spin excitations of $BaFe_2(As_{0.7}P_{0.3})_2$ obtained on MAPS with $E_i = 450$ meV. The negative scattering below ~50 meV is due to errors in background subtraction. Energy dependence of wave vector integrated [integration range is shown in the shaded box in the inset of (g)] dynamic susceptibility $\chi''(E)$ for (f) $BaFe_2As_2$ and (g) $BaFe_2(As_{0.7}P_{0.3})_2$. The vertical dashed lines in (d) and (e) show the wave vector integration range along the $[0,K]$ direction. (h) Energy dependence of the local dynamic spin susceptibility $\chi''(E)$ for $BaFe_2As_2$ (solid cyan line) and $BaFe_2(As_{0.7}P_{0.3})_2$ below (solid red triangle and solid red line) [35], the crystal structures of NaFeAs and $BaFe_2As_2$ are rather different, and it is still unclear that varying the iron-pnictogen distance within one family of iron pnictides can indeed control the electron correlations and spin excitation spectra.

In this paper, we present inelastic neutron scattering studies of the temperature and energy dependence of spin excitations in a $BaFe_2(As_{0.7}P_{0.3})_2$ superconductor ($T_c = 30$ K) [3,6]. We chose $BaFe_2(As_{0.7}P_{0.3})_2$ because it is the optimal isovalently doped $BaFe_2As_2$. At the same time, it has an average pnictogen height ($h_{Pn} = 1.28$ Å) significantly smaller than that of $BaFe_2As_2$ due to the smaller size of the P dopants [Figs. 1(b) and 1(c)] [4]. Since the average pnictogen height of $BaFe_2(As_{1-x}P_x)_2$ decreases continuously from $BaFe_2As_2$ to $BaFe_2(As_{0.7}P_{0.3})_2$ without modifying much the in-plane Fe-Fe distance or changing the valence of Fe [4], we expect weaker electron correlations and a wider spin excitation bandwidth in $BaFe_2(As_{0.7}P_{0.3})_2$ compared with that of $BaFe_2As_2$ [28].

Figures 1(d) and 1(e) show the energy dependence of $S(Q,E)$ of spin excitations for $BaFe_2As_2$ and $BaFe_2(As_{0.7}P_{0.3})_2$, respectively. While spin-wave dispersions of $BaFe_2As_2$ reach zone boundary positions $(1,\pm1)$ around 200 meV [Fig. 1(d)], dispersions of spin excitations of $BaFe_2(As_{0.7}P_{0.3})_2$ become steeper, and reach $(1,\pm1)$ at energies well above 200 meV [Fig. 1(e)]. Indeed, we find that spin excitations in $BaFe_2(As_{0.7}P_{0.3})_2$ have a lower intensity but a larger energy bandwidth than that of $BaFe_2As_2$ [30], as revealed in the energy dependence of the dynamic susceptibility $\chi''(E)$ integrated over the dashed vertical lines in Figs. 1(d) and 1(e) ($0.6 \leqslant H \leqslant 1.4$ and $0.6 \leqslant K \leqslant 1.4$) near the zone boundary $(1,\pm1)$ [Figs. 1(f) and 1(g)]. These results are also consistent with the energy dependence of the local dynamic susceptibility and DFT+DMFT calculations of $S(Q,E)$ [Figs. 1(h) and 2–4]. Therefore, the decreased average pnictogen height in $BaFe_2(As_{1-x}P_x)_2$ decreases the electron correlations and increases the overall spin excitation energy bandwidths.

## II. EXPERIMENTAL AND THEORETICAL RESULTS

Our neutron scattering experiments were carried out on the MAPS and 4SEASONS chopper spectrometers at ISIS, Rutherford Appleton Laboratory, U.K. and Japan Proton Accelerator Research Complex, Japan, respectively. Some measurements are also carried out on the EIGER triple-axis spectrometer at the Paul Scherrer Institut, Switzerland. Our $BaFe_2(As_{0.7}P_{0.3})_2$ single crystals were grown by a self-flux method [36]. For P-doped $BaFe_2(As_{1-x}P_x)_2$ near $x = 0.3$, the collinear static AF order in $BaFe_2As_2$ is suppressed and superconductivity reaches an optimal value at $T_c = 30$ K [37]. We coaligned ~17 g of single crystals in the $[H,H,L]$ scattering plane with a mosaic <7°. To facilitate easy comparison with spin waves in $BaFe_2As_2$, which has an orthorhombic AF ground state [30], we define the wave vector **Q** at

FIG. 1. (*Continued*) and above (open purple circles) $T_c$ with corrected magnetic form factor. Dashed cyan and red lines are DFT+DMFT calculations for $BaFe_2As_2$ and $BaFe_2(As_{0.7}P_{0.3})_2$, respectively.

$(q_x,q_y,q_z)$ in $\text{Å}^{-1}$ as $(H,K,L) = (q_x a/2\pi, q_y b/2\pi, q_z c/2\pi)$, where $a = b \approx 5.6$ Å and $c = 12.87$ Å using the orthorhombic magnetic unit cell notation where low-energy spin excitations are expected to stem from the in-plane wave vector positions $\mathbf{Q}_{\text{AF}} = (\pm 1,0)$ and $(0,\pm 1)$. For chopper spectrometer inelastic neutron scattering measurements, the incident beam energies were $E_i = 35$, 80, 250, and 450 meV at MAPS and $E_i = 13$, 21, 82, and 313 meV at 4SEASONS with $k_i$ parallel to the $c$ axis. Spin excitation intensity was normalized to absolute units using a vanadium standard (~30% error).

Since there is no evidence that the P dopant forms long-range order in $BaFe_2(As_{1-x}P_x)_2$, we use an effective pnictide position in the DFT+DMFT calculations to simulate the physical consequence of P doping. In $BaFe_2(As_{0.71}P_{0.29})_2$, the As and P heights are 1.332 and 1.151 Å from the Fe plane, respectively [38]. We therefore take an effective pnicogen height of 1.28 Å in our calculation, which is the average height of As and P in $BaFe_2(As_{0.71}P_{0.29})_2$ determined experimentally. This effective As/P height (1.28 Å) is less than the As height (1.36 Å) in the $BaFe_2As_2$ but substantially larger than the P height (1.19 Å) in the $BaFe_2P_2$.

In previous inelastic neutron scattering studies of low-energy spin excitations in powder [39] and single crystals [40] of optimally P-doped $BaFe_2(As_{1-x}P_x)_2$, a neutron spin resonance coupled to superconductivity has been identified similar to other iron-based superconductors [41–43]. A key conclusion of the work is that the energy of the resonance in $BaFe_2(As_{0.63}P_{0.34})_2$ is dispersive along the $c$ axis, indicating its close connection to the three-dimensional AF spin correlations [40]. In hole- and electron-doped $BaFe_2As_2$, the wave vector evolution of the low-energy spin excitations and the resonance can be well described by quasiparticle excitations through doping-dependent hole and electron Fermi surfaces [27,44]. Although substituting P for As in $BaFe_2(As_{1-x}P_x)_2$ is expected to be isovalent, angle-resolved photoemission spectroscopy (ARPES) experiments reveal changed hole and electron Fermi surfaces from $BaFe_2As_2$ to $BaFe_2(As_{0.7}P_{0.3})_2$ [45]. DFT+DMFT calculations also show that with increasing P doping, the hole Fermi surface with a dominating $d_{xy}$ orbital character shrinks whereas the hole Fermi surfaces with dominating $d_{xz}$ and $d_{yz}$ ($d_{z^2}$ near $k_z = \pi$) orbital characters expand and become more three dimensional along the $k_z$ direction [Figs. 2(a) and 2(b)]. However, the electron Fermi surfaces do not change significantly. Therefore, the electron-hole Fermi surface nesting condition becomes worse with P doping. This is consistent with the resulting changes in the wave vector dependence of spin excitations [Figs. 2(c) and 2(d)], where the low-energy spin excitations become weaker and more diffusive in the momentum space in $BaFe_2(As_{0.7}P_{0.3})_2$. Figures 2(e) and 2(f) show constant-$\mathbf{Q}$ scans at $\mathbf{Q} = (1,0,0)$ and $(1,0,1)$, respectively, below and above $T_c$. Consistent with previous work [40], we find that superconductivity-induced resonance is clearly dispersive, occurring at $E_{\text{res}} = 12$ meV at $\mathbf{Q} = (1,0,0)$ and $E_{\text{res}} = 9$ meV at $\mathbf{Q} = (1,0,1)$. Figures 2(g) and 2(h) summarize the energy dependence of the low-energy spin excitations at 40 K ($T \approx T_c + 10$ K) and 10 K ($T \approx T_c - 20$ K), respectively. Given the dispersive nature of the resonance, neutron time-of-fight measurements with a fixed incident energy and fixed sample rotation angle in Figs. 2(g) and 2(h) will probe a region of the excitation energies with different $L$ values. Figure 2(i) is a temperature difference plot, revealing a clear neutron spin resonance in the energy region of $E \approx 11$ meV and a spin gap below the resonance energy.

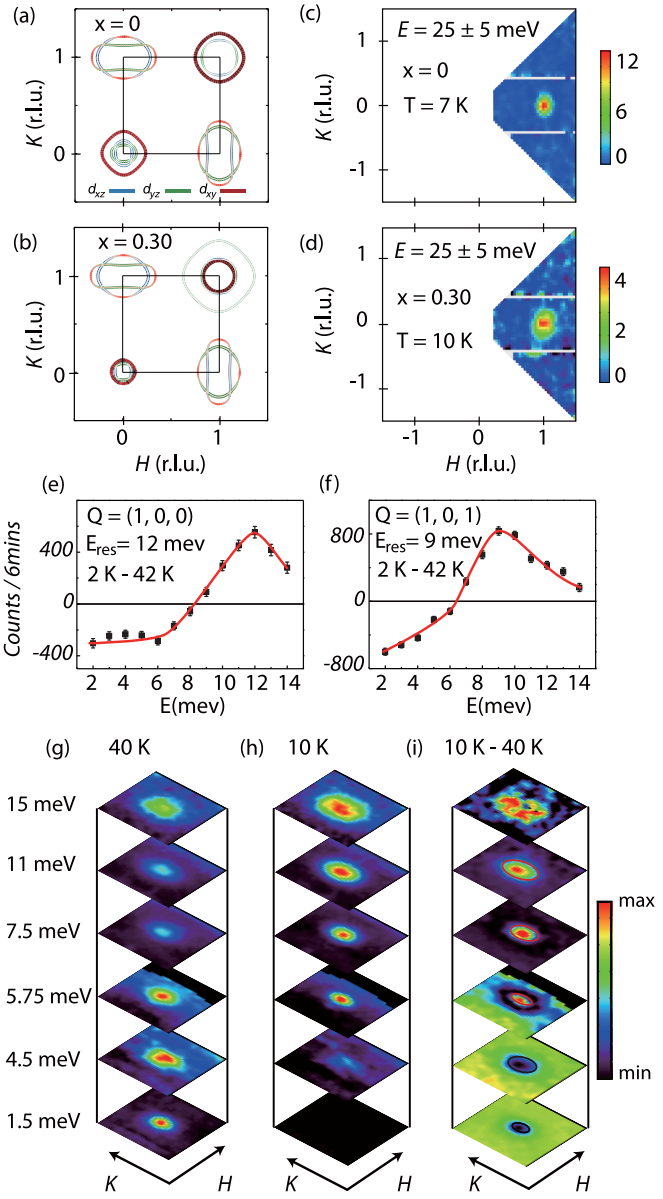


FIG. 2. (a), (b) Calculated Fermi surfaces of the $d_{xz}$, $d_{yz}$, and $d_{xy}$ orbitals for $BFe_2As_2$ and $BaFe_2(As_{0.7}P_{0.3})_2$, respectively. (c), (d) The corresponding wave vector dependence of the low-energy ($E =$ 25 meV) spin excitations. The color bars represent the vanadium-normalized absolute spin-wave intensity in units of mbar/sr/meV/Fe. The temperature differences of constant-wave vector scans at (e) $\mathbf{Q} = (1,0,0)$ and (f) $(1,0,1)$ below (2 K) and above (42 K) $T_c$ obtained using the EIGER triple-axis spectrometer. The modulation of resonance (superconductivity-induced intensity gain) with $L$ is consistent with previous experiments [40]. Constant-energy slices of the spin excitations as a function of increasing energy (g) at 40 K and (h) 10 K. (i) Temperature difference between 10 and 40 K, showing clearly the intensity gain in the energy region of 8–11 meV.

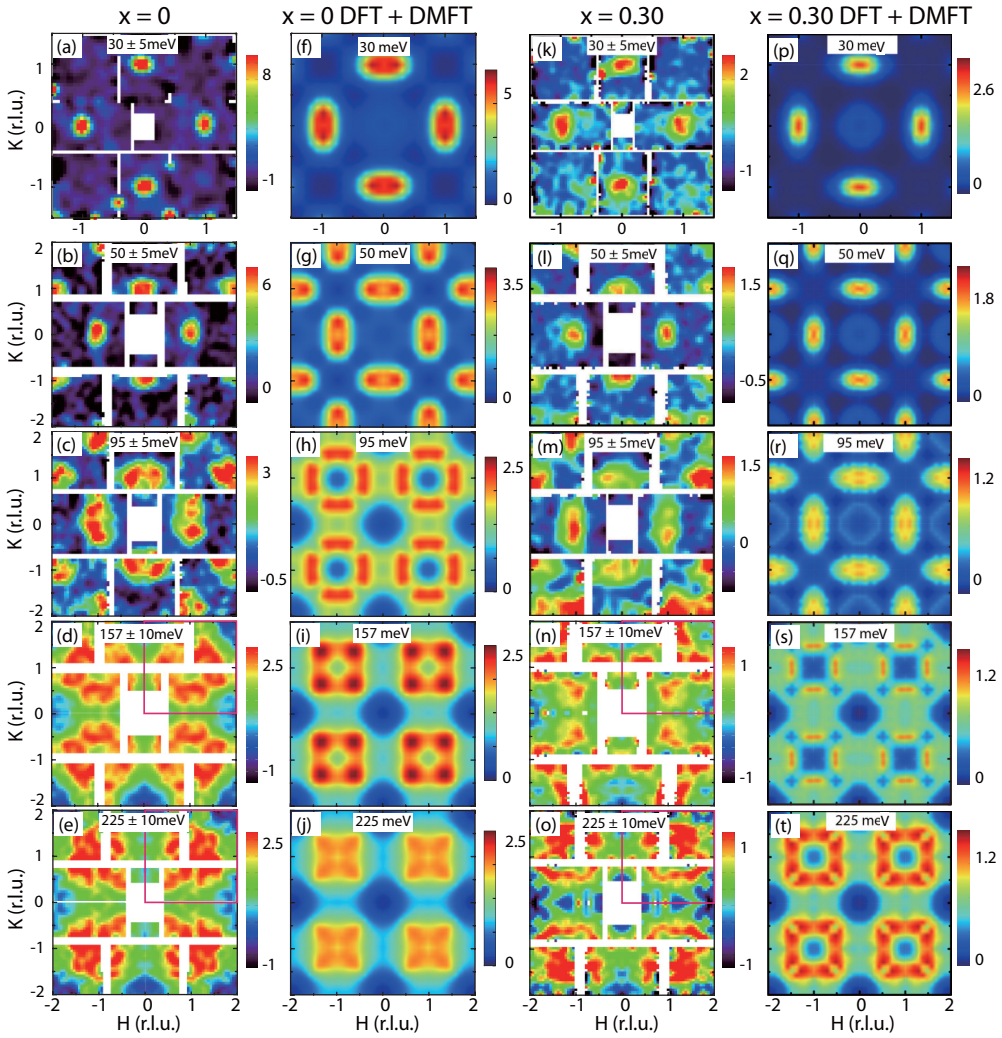


FIG. 3. Wave vector dependence of spin waves of $BaFe_2As_2$ at 7 K and spin excitations of $BaFe_2(As_{0.7}P_{0.3})_2$ at 10 K for energy transfers of (a), (k) $E = 30 \pm 5$ meV [$E_i = 80$ meV and $\mathbf{q} = (H,K,3)$]; (b), (i) $E = 50 \pm 5$ meV [$E_i = 250$ meV and $\mathbf{q} = (H,K,3)$]; (c), (m) $E = 95 \pm 5$ meV [$E_i = 250$ meV and $\mathbf{q} = (H,K,5)$]; (d), (n) $E = 157 \pm 10$ meV [$E_i = 450$ meV and $\mathbf{q} = (H,K,6)$]; (e), (o) $E = 225 \pm 10$ meV [$E_i = 450$ meV and $\mathbf{q} = (H,K,9)$]. In all cases, the $\pm$ meV indicates the energy integration range. The red boxes in (d), (e), (n), and (o) indicate regions that contain nonduplicate data from fourfold symmetrizing of the raw data (meaning only the data within the red box are statistically significant, and data in other regions of reciprocal space are mirror images of the red box data). (f)–(j) and (p)–(t) Calculations of identical energy slices from the DFT+DMFT method [46].

Assuming that isovalent P doping in $BaFe_2(As_{1-x}P_x)_2$ does not change the valence of Fe, the total moment sum rule requires the total magnetic spectral weight $M_0$, when integrated over all energy and momentum space [$M_0^2 = M^2 + \langle \mathbf{m}^2 \rangle = g^2 S(S+1)$, where $M$ is the static ordered moment, $\langle \mathbf{m}^2 \rangle$ is the local fluctuating moment, $g \approx 2$ is the Landé factor, and $S$ is the spin], to be independent of P doping [7]. From Figs. 2(c) and 2(d), we see a reduced low-energy spin excitation spectral weight in $BaFe_2(As_{0.7}P_{0.3})_2$ compared with $BaFe_2As_2$, as revealed by the DFT+DMFT calculation [Figs. 1(h) and 4].

Figures 3(a)–3(e) and 3(k)–3(o) compare the two-dimensional constant-energy ($E$) images of $S(Q,E)$ of spin waves of $BaFe_2As_2$ [30] and spin excitations of $BaFe_2(As_{0.7}P_{0.3})_2$ in the $(H,K)$ scattering plane at different energies. Figures 3(a)–3(e) show the evolution of spin waves of $BaFe_2As_2$ at energy transfers of $E = 30 \pm 5$, $50 \pm 5$, $95 \pm 5$, $157 \pm 10$, and $225 \pm 10$ meV, respectively. The corresponding spin excitations of $BaFe_2(As_{0.7}P_{0.3})_2$ are shown in Figs. 3(k)–3(o). At $E = 30 \pm 5$ [Figs. 3(a) and 3(k)] and $E = 50 \pm 5$ meV [Figs. 3(b) and 3(l)], spin excitations in $BaFe_2(As_{0.7}P_{0.3})_2$ form transversely elongated ellipses centered at the in-plane AF zone centers $(\pm 1,0)$ and $(0,\pm 1)$ of the undoped $BaFe_2As_2$, but with considerably lower intensity. On increasing the energies to $E = 95 \pm 5$ meV [Fig. 3(m)], spin excitations of $BaFe_2(As_{0.7}P_{0.3})_2$ begin to split transversely from $(\pm 1,0)$, similar to that of spin waves of $BaFe_2As_2$ [Fig. 3(c)]. On further increasing the energy to $E = 157 \pm 10$ [Fig. 3(n)] and $E = 225 \pm 10$ meV [Fig. 3(o)], spin excitations of $BaFe_2(As_{0.7}P_{0.3})_2$ form anisotropic rings centered around $(\pm 1,\pm 1)$. Figures 3(d) and 3(e) show spin waves of $BaFe_2As_2$ at $E = 157 \pm 10$ and $E = 225 \pm 10$ meV, respectively. We see that spin waves of $BaFe_2As_2$ at $E = 225 \pm 10$ meV nearly form a solid spot at $(\pm 1,\pm 1)$, suggesting that the system has

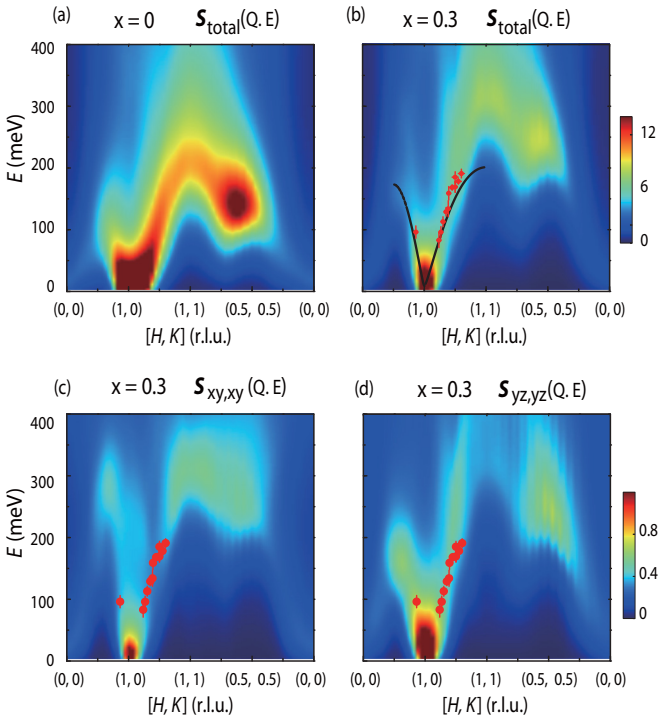


FIG. 4. (a) Calculated total dynamic magnetic structure factor $S(Q,E)$ for (a) $BaFe_2As_2$ and (b) $BaFe_2(As_{0.7}P_{0.3})_2$ using DFT+DMFT. The solid red points in (b) are data from cuts to Fig. 3 and the solid line is the dispersion of $BaFe_2As_2$ from Ref. [30]. (c), (d) Calculated dynamic magnetic structure factors from the $d_{xy}$-$d_{xy}$ and $d_{yz}$-$d_{yz}$ intraorbital contributions, respectively.

already reached the zone boundary at this energy. For comparison, spin excitations of $BaFe_2(As_{0.7}P_{0.3})_2$ at $E = 225 \pm 10$ meV still have a ring structure near $(\pm 1, \pm 1)$ [Fig. 3(o)], as confirmed by a comparison of constant-energy cuts across the data (see Supplemental Fig. 5 in Ref. [46]). These results suggest a higher zone boundary energy for $BaFe_2(As_{0.7}P_{0.3})_2$.

To quantitatively compare the experimental results with a combined DFT+DMFT theory [28], we show in Figs. 3(f)–3(j) and 3(p)–3(t) the calculated wave vector dependence of spin excitations of $BaFe_2As_2$ and $BaFe_2(As_{0.7}P_{0.3})_2$, respectively, at energies in Figs. 3(a)–3(e) [28]. We see that spin excitations at different energies obtained from the DFT+DMFT calculation in Figs. 3(p)–3(t) have many similarities with the experimental data [Figs. 3(k)–3(o)].

Figures 4(a) and 4(b) show the calculated dynamical magnetic structure factor $S(Q,E)$ for $BaFe_2As_2$ and $BaFe_2(As_{0.7}P_{0.3})_2$, respectively. Our calculation reveals a considerable magnetic spectral weight for energies above 300 meV for both samples, contrasting to the vanishing local dynamic susceptibility for energies above 300 meV in $BaFe_2As_2$ [Fig. 1(h)] [47]. The experimentally determined spin excitation dispersion along the $[1, K]$ direction for $BaFe_2(As_{0.7}P_{0.3})_2$ is well captured by the DFT+DMFT calculations [Fig. 4(b)]. For comparison, we also plot in Fig. 4(b) the experimentally determined dispersion along the same direction for $BaFe_2As_2$ as a solid line [30]. To understand the different orbital contributions to the spin excitations, we show in Figs. 4(c) and 4(d) the $d_{xy}$-$d_{xy}$ and $d_{yz}$-$d_{yz}$ intraorbital contribution to the dynamic susceptibility. We see that low-energy spin excitations near (1,0) are mostly contributed by excitations involving the $d_{yz}$ orbital, while high-energy spin excitations around 300 meV near (1,1) come mostly from excitations related to the $d_{xy}$ orbital. This is in stark contrast with spin excitations in the Co-doped LiFeAs compound, where the low-energy spin excitations are dominated by contributions from the $d_{xy}$ orbital [48]. In Ref. [48], it was concluded that the $d_{xz/yz}$ orbitals play an important role in the superconductivity of LiFeAs since their absence in $LiFe_{0.88}Co_{0.12}As$ suppresses superconductivity. The strong low-energy spin excitations contributed by the $d_{yz/xz}$ orbitals in $BaFe_2(As_{0.7}P_{0.3})_2$ shown in Fig. 4(d) suggest that the nesting of the $d_{yz/xz}$ orbitals is good for high-temperature superconductivity.

Figure 1(h) compares the energy dependence of the local dynamic spin susceptibility for $BaFe_2As_2$, $BaFe_2(As_{0.7}P_{0.3})_2$, and DFT+DMFT calculated values. We see that the peak for local dynamic spin susceptibility for $BaFe_2(As_{0.7}P_{0.3})_2$ occurs around 220 meV, while it is around 180 meV for $BaFe_2As_2$. These results are consistent with energy cuts near the zone boundary for these materials shown in Figs. 1(f) and 1(g). The total fluctuating magnetic moments for $BaFe_2(As_{0.7}P_{0.3})_2$ and $BaFe_2As_2$ are $\langle m^2 \rangle \approx 1.6 \pm 0.2$ (below $\sim$250 meV) and $3.6\mu_B^2$ per Fe, respectively [47]. This means that the fluctuating moments of $BaFe_2(As_{0.7}P_{0.3})_2$ are smaller than those of $BaFe_2As_2$ within our energy integration region, consistent with the presence of more magnetic spectral weight at higher energies or a reduced fluctuating moment. These results thus suggest that the decreased iron-pnictogen height in iron pnictides from $BaFe_2As_2$ to $BaFe_2(As_{0.7}P_{0.3})_2$ increases the spin excitation bandwidth and decreases the electron correlation effects. Since the reduced pnicogen height due to P doping increases indirect hopping between Fe $3d$ orbitals and pnicogen $p$ orbitals, and weakens the kinetic frustration as direct hopping between Fe $3d$ orbitals remains almost the same as the Fe-Fe distance changes negligibly with P doping, the bandwidths of the Fe $3d$ orbitals increase with increasing P doping [46] and the electronic correlation effects decrease. The increased bandwidths lead to a reduction of the one-particle Green's function, and thus a reduction in the bare two-particle susceptibility. Neglecting the change in the two-particle vertex function due to P doping, this reduction in the bare two-particle susceptibility is responsible for the reduced low-energy spin excitation intensity. Similarly, the spin excitation bandwidths increase due to the reduced pnicogen height in $BaFe_2(As_{0.7}P_{0.3})_2$.

The reduction of the pnicogen height in $BaFe_2(As_{0.7}P_{0.3})_2$ from $BaFe_2As_2$ reduces the low-energy spin excitation intensity centered at $Q_{AF}$ and eliminates the static long-range AF order in the undoped $BaFe_2As_2$. At the same time, the pnicogen height in $BaFe_2(As_{0.7}P_{0.3})_2$ is still high enough to maintain an intermediate electronic correlation strength with sufficient low-energy spin fluctuations to mediate superconductivity. For spin excitation mediated superconductors [5], superconductivity is controlled by the effective magnetic exchange coupling $J$ and the strength of the electron-spin excitation coupling [27]. Since the effective magnetic exchange couplings in $BaFe_2(As_{0.7}P_{0.3})_2$ are considerably larger than those of the $BaFe_2As_2$, it would be interesting to compare superconductivity-induced changes in spin excitations

of $BaFe_2(As_{0.7}P_{0.3})_2$ and electron/hole-doped $BaFe_2As_2$ [27]. By comparing the absolute intensity changes of the resonance below and above $T_c$, we find that spin excitations changes across $T_c$ are still much larger than the superconducting condensation energy [46,49], thus supporting the notion that magnetism is crucial for the superconductivity of $BaFe_2(As_{0.7}P_{0.3})_2$.

## III. CONCLUSIONS

In summary, we have used inelastic neutron scattering to map out spin excitations of isovalently doped $BaFe_2(As_{0.7}P_{0.3})_2$. By comparing spin excitations of this material with those of $BaFe_2As_2$ and DFT+DMFT calculations, we conclude that the iron-pnictogen height in iron pnictides directly controls the spin excitation bandwidth and electron correlations. These results are consistent with the idea that electron correlations in iron-based superconductors arise primarily from the Hund's coupling $J_H$, and low-energy spin excitations are consequences of nesting between hole and electron Fermi surfaces.

## ACKNOWLEDGMENTS

The work at IOP, CAS is supported by National Natural Science Foundation of China (NSFC Projects: 11374011, 11374346, 11674406 and 11611130165), the Ministry of Science and Technology of China (973 projects: 2012CB821400 and 2015CB921302), and the Strategic Priority Research Program (B) of CAS (Grant No. XDB07020300). H. Luo is grateful for the support from the Youth Innovation Promotion Association, CAS (No. 2016004). Neutron scattering work at Rice is supported by the U.S. DOE, Office of Basic Energy Sciences, under Contract No. DE-SC0012311. Part of the materials work at Rice University is supported by the Robert A. Welch Foundation Grant No. C-1839. The neutron experiment at the Materials and Life Science Experimental Facility of J-PARC was performed under a user program (Proposal No. 2014B0277). The computational works at Rice and Rutgers are supported by NSF DMREF DMR-1436006 and DMR-1435918, respectively. Experiments at the ISIS Pulsed Neutron and Muon Source were supported by a beam time allocation from the Science and Technology Facilities Council.

[1] Y. Kamihara, T. Watanabe, M. Hirano, and H. Hosono, J. Am. Chem. Soc. **130**, 3296 (2008).
[2] C. de la Cruz, Q. Huang, J. W. Lynn, J. Li, W. Ratcliff, II, J. L. Zarestky, H. A. Mook, G. F. Chen, J. L. Luo, N. L. Wang, and P. C. Dai, Nature (London) **453**, 899 (2008).
[3] S. Jiang, H. Xing, G. Xuan, C. Wang, Z. Ren, C. Feng, J. Dai, Z. Xu, and G. Cao, J. Phys.: Condens. Matter **21**, 382203 (2009).
[4] D. C. Johnston, Adv. Phys. **59**, 803 (2010).
[5] D. J. Scalapino, Rev. Mod. Phys. **84**, 1383 (2012).
[6] T. Shibauchi, A. Carrington, and Y. Matsuda, Annu. Rev. Condens. Matter Phys. **5**, 113 (2014).
[7] P. C. Dai, Rev. Mod. Phys. **87**, 855 (2015).
[8] P. A. Lee, N. Nagaosa, and X.-G. Wen, Rev. Mod. Phys. **78**, 17 (2006).
[9] P. J. Hirschfeld, M. M. Korshunov, and I. I. Mazin, Rep. Prog. Phys. **74**, 124508 (2011).
[10] A. Chubukov, Annu. Rev. Condens. Matter Phys. **3**, 57 (2012).
[11] Q. Si and E. Abrahams, Phys. Rev. Lett. **101**, 076401 (2008).
[12] C. Fang, H. Yao, W. F. Tsai, J. P. Hu, and S. A. Kivelson, Phys. Rev. B **77**, 224509 (2008).
[13] C. Xu, M. Muller, and S. Sachdev, Phys. Rev. B **78**, 020501(R) (2008).
[14] D. N. Basov and A. V. Chubukov, Nat. Phys. **7**, 272 (2011).
[15] K. Haule and G. Kotliar, New J. Phys. **11**, 025021 (2009).
[16] Z. P. Yin, K. Haule, and G. Kotliar, Nat. Mater. **10**, 932 (2011).
[17] A. Goerges, L. de' Medici, and J. Mravlje, Annu. Rev. Condens. Matter Phys. **4**, 137 (2013).
[18] C. C. Lee, W. G. Yin, and W. Ku, Phys. Rev. Lett. **103**, 267001 (2009).
[19] F. Krüger, S. Kumar, J. Zaanen, and J. van den Brink, Phys. Rev. B **79**, 054504 (2009).
[20] W. C. Lv, J. S. Wu, and P. Phillips, Phys. Rev. B **80**, 224506 (2009).
[21] C.-C. Chen, J. Maciejko, A. P. Sorini, B. Moritz, R. R. P. Singh, and T. P. Devereaux, Phys. Rev. B **82**, 100504(R) (2010).
[22] B. Valenzuela, E. Bascones, and M. J. Calderón, Phys. Rev. Lett. **105**, 207202 (2010).
[23] G. Kotliar, S. Y. Savrasov, K. Haule, V. S. Oudovenko, O. Parcollet, and C. A. Marianetti, Rev. Mod. Phys. **78**, 865 (2006).
[24] K. Haule, C.-H. Yee, and K. Kim, Phys. Rev. B **81**, 195107 (2010).
[25] M. S. Liu, L. W. Harriger, H. Q. Luo, M. Wang, R. A. Ewings, T. Guidi, H. Park, K. Haule, G. Kotliar, S. M. Hayden, and P. C. Dai, Nat. Phys. **8**, 376 (2012).
[26] H. Park, K. Haule, and G. Kotliar, Phys. Rev. Lett. **107**, 137007 (2011).
[27] M. Wang, C. L. Zhang, X. Y. Lu, G. T. Tan, H. Q. Luo, Y. Song, M. Y. Wang, X. T. Zhang, E. A. Goremychkin, T. G. Perring, T. A. Maier, Z. P. Yin, K. Haule, G. Kotliar, and P. C. Dai, Nat. Commun. **4**, 2874 (2013).
[28] Z. P. Yin, K. Haule, and G. Kotliar, Nat. Phys. **10**, 845 (2014).
[29] S. O. Diallo, V. P. Antropov, T. G. Perring, C. Broholm, J. J. Pulikkotil, N. Ni, S. L. Bud'ko, P. C. Canfield, A. Kreyssig, A. I. Goldman, and R. J. McQueeney, Phys. Rev. Lett. **102**, 187206 (2009).
[30] L. W. Harriger, H. Q. Luo, M. S. Liu, C. Frost, J. P. Hu, M. R. Norman, and P. C. Dai, Phys. Rev. B **84**, 054544 (2011).
[31] R. A. Ewings, T. G. Perring, J. Gillett, S. D. Das, S. E. Sebastian, A. E. Taylor, T. Guidi, and A. T. Boothroyd, Phys. Rev. B **83**, 214519 (2011).
[32] J. T. Park, G. Friemel, T. Loew, V. Hinkov, Yuan Li, B. H. Min, D. L. Sun, A. Ivanov, A. Piovano, C. T. Lin, B. Keimer, Y. S. Kwon, and D. S. Inosov, Phys. Rev. B **86**, 024437 (2012).
[33] H. Q. Luo, X. Y. Lu, R. Zhang, M. Wang, E. A. Goremychkin, D. T. Adroja, S. Danilkin, G. Deng, Z. Yamani, and P. C. Dai, Phys. Rev. B **88**, 144516 (2013).

[34] S. L. Li, C. de la Cruz, Q. Huang, G. F. Chen, T.-L. Xia, J. L. Luo, N. L. Wang, and P. C. Dai, Phys. Rev. B **80**, 020504(R) (2009).
[35] C. L. Zhang, L. W. Harriger, Z. P. Yin, W. C. Lv, M. Y. Wang, G. T. Tan, Y. Song, D. L. Abernathy, W. Tian, T. Egami, K. Haule, G. Kotliar, and P. C. Dai, Phys. Rev. Lett. **112**, 217202 (2014).
[36] D. Hu, X. Y. Lu, W. L. Zhang, H. Q. Luo, S. L. Li, P. P. Wang, G. F. Chen, F. Han, S. R. Banjara, A. Sapkota, A. Kreyssig, A. I. Goldman, Z. Yamani, Ch. Niedermayer, M. Skoulatos, R. Georgii, T. Keller, P. S. Wang, W. Q. Yu, and P. C. Dai, Phys. Rev. Lett. **114**, 157002 (2015).
[37] J. M. Allred, K. M. Taddei, D. E. Bugaris, S. Avci, D. Y. Chung, H. Claus, C. de la Cruz, M. G. Kanatzidis, S. Rosenkranz, R. Osborn, and O. Chmaissem, Phys. Rev. B **90**, 104513 (2014).
[38] M. Rotter, C. Hieke, and D. Johrendt, Phys. Rev. B **82**, 014513 (2010).
[39] M. Ishikado, Y. Nagai, K. Kodama, R. Kajimoto, M. Nakamura, Y. Inamura, S. Wakimoto, H. Nakamura, M. Machida, K. Suzuki, H. Usui, K. Kuroki, A. Iyo, H. Eisaki, M. Arai, and S. I. Shamoto, Phys. Rev. B **84**, 144517 (2011).
[40] C. H. Lee, P. Steffens, N. Qureshi, M. Nakajima, K. Kihou, A. Iyo, H. Eisaki, and M. Braden, Phys. Rev. Lett. **111**, 167002 (2013).
[41] M. D. Lumsden, A. D. Christianson, D. Parshall, M. B. Stone, S. E. Nagler, G. J. MacDougall, H. A. Mook, K. Lokshin, T. Egami, D. L. Abernathy, E. A. Goremychkin, R. Osborn, M. A. McGuire, A. S. Sefat, R. Jin, B. C. Sales, and D. Mandrus, Phys. Rev. Lett. **102**, 107005 (2009).
[42] S. Chi, A. Schneidewind, J. Zhao, L. W. Harriger, L. Li, Y. Luo, G. Cao, Z. Xu, M. Loewenhaupt, J. Hu, and P. C. Dai, Phys. Rev. Lett. **102**, 107006 (2009).
[43] D. S. Inosov, J. T. Park, P. Bourges, D. L. Sun, Y. Sidis, A. Schneidewind, K. Hradil, D. Haug, C. T. Lin, B. Keimer, and V. Hinkov, Nat. Phys. **6**, 178 (2010).
[44] H. Q. Luo, Z. Yamani, Y. C. Chen, X. Y. Lu, M. Wang, S. L. Li, T. A. Maier, S. Danilkin, D. T. Adroja, and P. C. Dai, Phys. Rev. B **86**, 024508 (2012).
[45] Y. Zhang, Z. R. Ye, Q. Q. Ge, F. Chen, Juan Jiang, M. Xu, B. P. Xie, and D. L. Feng, Nat. Phys. **8**, 371 (2012).
[46] See Supplemental Material at http://link.aps.org/supplemental/10.1103/PhysRevB.94.094504 for additional data and analysis.
[47] L. W. Harriger, M. S. Liu, H. Q. Luo, R. A. Ewings, C. D. Frost, T. G. Perring, and P. C. Dai, Phys. Rev. B **86**, 140403(R) (2012).
[48] Yu Li, Z. P. Yin, X. C. Wang, D. W. Tam, D. L. Abernathy, A. Podlesnyak, C. L. Zhang, M. Wang, L. Y. Xing, C. Q. Jin, K. Haule, G. Kotliar, T. A. Maier, and P. C. Dai, Phys. Rev. Lett. **116**, 247001 (2016).
[49] Z. Diao, D. Campanini, L. Fang, W.-K. Kwok, U. Welp, and A. Rydh, Phys. Rev. B **93**, 014509 (2016).